NJC

Accepted Manuscript

This is an *Accepted Manuscript*, which has been through the Royal Society of Chemistry peer review process and has been accepted for publication.

Accepted Manuscripts are published online shortly after acceptance, before technical editing, formatting and proof reading. Using this free service, authors can make their results available to the community, in citable form, before we publish the edited article. We will replace this *Accepted Manuscript* with the edited and formatted *Advance Article* as soon as it is available.

You can find more information about *Accepted Manuscripts* in the Information for Authors.

Please note that technical editing may introduce minor changes to the text and/or graphics, which may alter content. The journal's standard Terms & Conditions and the Ethical guidelines still apply. In no event shall the Royal Society of Chemistry be held responsible for any errors or omissions in this *Accepted Manuscript* or any consequences arising from the use of any information it contains.

ROYAL SOCIETY OF CHEMISTRY

www.rsc.org/njc

Journal Name

RSCPublishing

ARTICLE

Rattle-type $NiCo_2O_4$-carbon composite microspheres as electrode materials for high-performance supercapacitors

Cite this: DOI: 10.1039/xoxxoooooox

Yongchao Ma[a], Haiyan Jiang[a], Qingzhi Liu[a], Wukui Kang[a] and Jinsheng Shi[a]*

Received ooth January 2012,
Accepted ooth January 2012

DOI: 10.1039/xoxxoooooox

www.rsc.org/

In this work, $NiCo_2O_4$-carbon composite microspheres with rattle-type structure were successfully prepared by a template-engaged hydrothermal and subsequent calcination treatment. These rattle-type microspheres are composed of a solid carbon core and a porous shell with nanorods as building blocks. The calcination temperature of the $NiCo_2O_4$-carbon precursor has an obvious affect upon the morphology as well as the resultant capacitive performances. Because of the unique structure and high specific surface area, these rattle-type $NiCo_2O_4$-carbon composite microspheres exhibited excellent electrochemical performances with high specific capacitance (790 F g^{-1} at 1 A g^{-1}), and even kept it as high as 609 F g^{-1} at 10 A g^{-1}. Additionally, excellent cycling stability with 99.4 % specific capacitance retention after continuous 2000 cycles at a current density of 2 A g^{-1} was observed, suggesting their promising application in supercapacitors. The synergistic effect of different components and the rattle-type structure may contribute to the outstanding performance of the composite electrode.

1. Introduction

The ability to fabricate the novel nano/microstructures with controllable structure, size, and shape has attracted great interest because of the strong correlation between the structure, shape and size of the nano/microstructures and their fascinating physical/chemical properties[1-3]. As a unique class of structured materials, the rattle-type structure has attracted increasing research attention owing to their potential application in drug delivery[4], catalyst[5], lithium-ion batteries[6], and gas sensors[7, 8]. So far, a variety of synthesis methods have been developed to prepare these special structures. Kaskel et al. have reported the synthesis of rattle-type Fe_3O_4@SiO_2 hollow mesoporous spheres by using the colloidal carbon spheres as the templates[9]. Furthermore, Jiao and co-workers have described an environmentally friendly and template-free route to prepare rattle-type TiO_2 hollow microspheres[10]. In addition, Mishima et al. have recently prepared magnetic rattle-type particles by using sol-gel reactions in a water-in-oil emulsion[11]. However, the striking feature for most of these tattle-type structures is that their shells are generally composed of or aggregated from numerous nanoparticles with an irregular arrangement. Recent reports show that orientated self-assembled or self-supported structure can help to enhance electrochemical performance[12, 13]. Although much progress has been made in the synthesis of rattle-type structures, the fabrication of rattle-type nano/microspheres with self-assembled oriented shell still remains a great challenge.

Supercapacitor has been considered as one of the most promising energy storage devices because of their many advantages, including high power density, faster charge and discharge processes, longer lifespan etc[14-16]. Transition metal oxides have been widely used as active electrode materials in supercapacitors[17, 18]. Among them, spinel $NiCo_2O_4$ has been regarded as a promising electrode material, due to its intriguing properties, such as good conductivity, environmental friendly and highly reversible redox reactions[19-21]. Various nano/microstructures of $NiCo_2O_4$, such as flower-like spheres[22], nanosheets[23], hollow microspheres[24] and mesoporous nanoparticles[25], have been prepared to improve the electrochemical properties. The results show that the fine control size and morphology is an efficient way to optimize the electrochemical performance of the $NiCo_2O_4$ electrodes[26]. However, to the best of our knowledge, works focused on the preparation of rattle-type $NiCo_2O_4$ microspheres with self-assembled oriented shell are really few.

Herein, we report a facile template-mediated hydrothermal and subsequent calcination process for the fabrication of rattle-type $NiCo_2O_4$-carbon microstructures. The shell of the composite microspheres was composed of nanorods. The effect of calcination temperature of the $NiCo_2O_4$-carbon precursor on the morphology and electrochemical performance has been investigated in detail. The rattle-type $NiCo_2O_4$-carbon microstructures exhibited excellent electrochemical performance with a high specific capacity and good cycling stability.

2. Experimental

2.1. Materials and chemicals

All the reagents were purchased from Sinopharm Chemical Reagent Beijing Co., Ltd., and used without any further purification.

2.2. Preparation of carbon spheres

The carbon microspheres were synthesized through the carbonization of glucose under hydrothermal conditions. In a typical experiment[27], 8 g of glucose was dissolved in 60 mL distilled water to form a clear solution. Then the resulting solution was added into a 100 mL polytetrafluoroethylene (PTFE) Teflon-lined autoclave. After 7 h of hydrothermal treatment at 190 ℃, the obtained black-brown precipitate was centrifuged, washed with distilled water and ethanol three times, and then dried at 80 °C overnight.

2.3. Synthesis of rattle-type $NiCo_2O_4$–carbon composite microspheres

In a typical procedure, the obtained carbon spheres were added into 60 mL distilled water. In order to completely disperse the carbon spheres, the breaker was place in an ultrasonic bath for 30 min. Then, 3 mmol of $Ni(NO_3)_2{\cdot}6H_2O$, 6 mmol of $Co(NO_3)_2{\cdot}6H_2O$ and 3.16 g of urea were dissolved into the above mixture at the room temperature under vigorous magnetic stirring. After being stirred for 30 min, the as-obtained solution was transferred into a 100 mL polytetrafluoroethylene (PTFE) Teflon-lined autoclave and maintained at 120 ℃ for 6 h. After being cooled to room temperature naturally, the $NiCo_2O_4$-carbon precursor was collected by centrifugation and washed with distilled water and ethanol several times in sequence, and then dried at 80 ℃ overnight. In order to obtain rattle-type $NiCo_2O_4$-carbon composite microspheres, the as-grown $NiCo_2O_4$-carbon precursors were annealed in air for 3 h at 250 ℃ with a ramp rate of 5 ℃ min^{-1}. In order to investigate the effect of calcination temperature on the structure and electrochemical properties, the $NiCo_2O_4$-carbon precursors were calcinated at 300 ℃, 400 ℃ and 500 ℃ for 3 h in air, respectively.

2.4. Characterization

The purity and crystallite structure of the as-obtained samples were characterized using X-ray powder diffraction (XRD) (Bruker, D8-Advance XRD) with Cu Kα radiation (λ =0.15148 nm) operating at 30.0 kV and 20.0 mA. The thermal behavior of the precursor was examined by thermogravimetric (TG) and differential thermal analysis (DTA) on a Henven HCT-2 thermal analyzer (Beijing, China) with a ramp rate of 10 ℃ min^{-1} from room temperature to 700 °C in air. Field emission scanning electron microscopy (FESEM) images were acquired on a Hitachi S4800 scanning electron microscope (Tokyo, Japan) to examine the morphology of the products. Morphologies of the detailed structures were measured with a FEI Tecnai G220 high-resolution transmission electron microscope (TEM) (Hillsboro, OR, USA). The specific surface areas, pore size, and pore volume of the resultant products were further investigated by nitrogen adsorption/desorption measurements at 77K on a NOVA 2200e analyzer.

2.5. Electrochemical Measurement

For the electrochemical measurements, the as-prepared sample was mixed with acetylene black as the conducting material and polytetrafluoroethylene (PTFE) binder, in a weight ratio of 80:15:5. A small amount of distilled water was then added to make more homogeneous mixture. Then, the slurries were coated on the nickel foam substrates (1.0 cm × 1.0 cm). After being dried at 80 ℃ for 2 h, the as-formed electrodes loaded with the active material were then pressed at 14 MPa. The obtained $NiCo_2O_4$ modified electrode was then used as a working electrode. A platinum plate (1 cm^2) and saturated calomel electrode (SCE) were used as a counter electrode and reference electrode, respectively. The electrolyte was a 3 M KOH aqueous solution. The electrochemical measurements were conducted in a three compartment cell using a LAND battery test instrument (CT2001A, Wuhan, China). Cyclic voltammetry (CV) was conducted by LK2005A electrochemical workstation with scan rates of 2 mV s^{-1}, 5 mV s^{-1}, 10 mV s^{-1}, 20 mV s^{-1} and 30 mV s^{-1}. The galvanostatic charge−discharge (CD) tests were conducted at the currents of 1 A g^{-1}, 2 A g^{-1}, 4 A g^{-1}, 8 A g^{-1} and 10 A g^{-1}. The electrochemical impedance spectroscopy (EIS) measurements were carried out by applying an AC voltage with 5 mV amplitude in a frequency range from 0.01 Hz to 100 kHz at open circuit potential.

The specific capacitance (C, F g^{-1}), energy density (E, Wh kg^{-1}), and power density (P, W kg^{-1}) were calculated from the galvanostatic CD curves based on the following equation[28]:

$$C = \frac{It_D}{\Delta V} \quad (1)$$

$$\mathrm{E} = \frac{1}{2}\mathrm{C}(\Delta \mathrm{V})^2 \quad (2)$$

$$P = \frac{E}{t_D} \quad (3)$$

where I, t_D, and ΔV are the discharging current density (A g^{-1}), the discharging time (s), and the discharging potential range (V), respectively. In addition, columbic efficiency (η) of the electrodes was evaluated according to the following equation[29]:

$$\eta = \frac{t_D}{t_C} \times 100\% \quad (4)$$

where t_D and t_C are the discharging and charging time, respectively.

3. Results and discussion

3.1 Physicochemical characterization

The first step of the synthesis process involved the production of uniform carbon microspheres according to the previous study[27]. Fig. S1a is the FESEM image of the as-prepared carbon spheres, showing the spherical geometry with the diameter of about 1.5 μm. Besides, the XRD pattern (Fig. S1b) confirmed the amorphous nature of the carbon microsphere.

TG and DTA measurements were performed to assess the follow-up calcination process of the as-prepared $NiCo_2O_4$ precursors. As shown in Fig. 1, the weight loss occurring from 50 ℃ to 250 ℃ is assigned to the evaporation of free water. However, above 250 ℃, two weight loss steps are obvious: the former range from 250 ℃ to 300 ℃ is attributed to the decomposition of the outer part of carbon templates, owing to the exposure of them in air[30]. Meanwhile, the precursor was decomposed and the $NiCo_2O_4$ samples were formed[31]. Besides, the latter weight loss from 300 ℃ to 400 ℃ may be ascribed

to continuing combustion of template, resulting in the exothermic peak from 300 ℃ to 400 ℃ (Fig. S2). This may be explained by the fact that the carbonized core of the carbon spheres has the greater binding energy than that of surface material in the carbon spheres[27, 32].

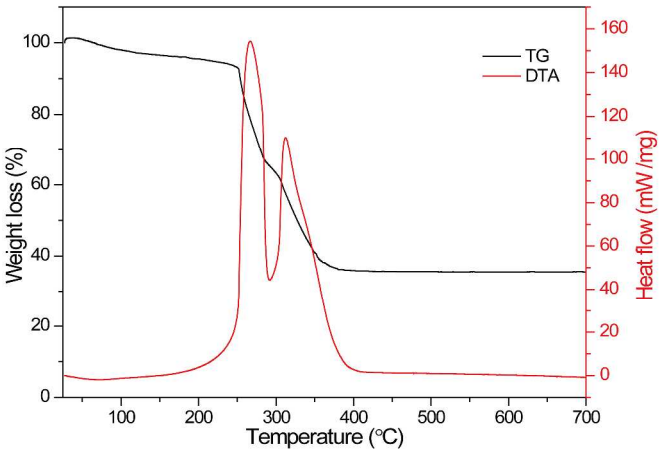

Fig. 1 TG and DTA curves of the as-synthesized $NiCo_2O_4$ precursor.

The purity and crystalline phase of the as-fabricated $NiCo_2O_4$ products were studied by the XRD analysis. Fig. 2 shows the typical XRD patterns of the sample obtained by calcinating $NiCo_2O_4$ precursor at various temperatures. It can be observed from the Fig. 2a that the $NiCo_2O_4$ phase is completely formed at 250 ℃, which can be well indexed to the spinel $NiCo_2O_4$ crystalline structure (JCPDS no. 20-0781). The broad diffraction peaks with relatively lower intensities are may attributed to the small size of the $NiCo_2O_4$ articles and the poor crystallinity of carbon species[33]. Besides, there are no diffraction peaks from any other impurities, indicating the high quality of the as-obtained samples. In Fig. 2b, the crystallinity of products enhanced with the raising calcination temperature. In the previous report, the decomposition temperature of $NiCo_2O_4$ occurs at about 400 ℃[34]. However, in the present study, the XRD pattern (Fig. 2c) remains almost unchanged even at 400 ℃, which indicated the higher thermal stability. Furthermore, as shown in Fig. 2d, when increasing the calcination temperature to 500 ℃, $NiCo_2O_4$ coexisting with cubic NiO (JCPDS no. 65-2901) as impurity phase was emerged. These results confirmed the fact that higher calcination temperature can lead to the decomposition of $NiCo_2O_4$ sample[35].

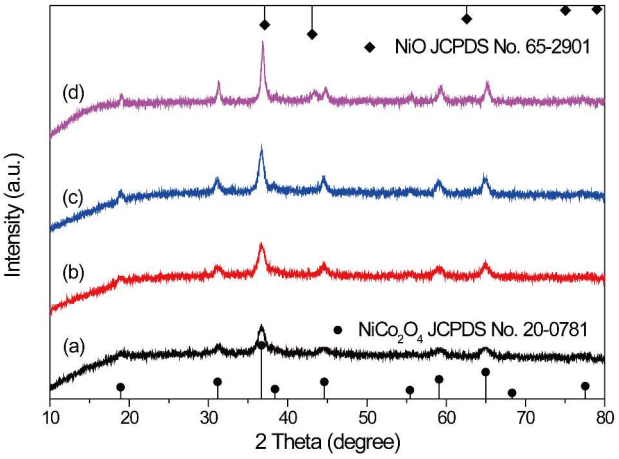

Fig. 2 XRD patterns of the as-synthesized $NiCo_2O_4$ products obtained by different calcination temperatures of the precursor: (a) 250 ℃, (b) 300 ℃, (c) 400 ℃ and (d) 500 ℃.

The morphologies of the $NiCo_2O_4$-carbon precursors and $NiCo_2O_4$-carbon rattle-type composite microspheres were characterized by SEM. Fig. 3a is the SEM image of the $NiCo_2O_4$-carbon precursors with a diameter of about 2-5 μm. It can be clearly seen the urchin-like hierarchical structures were uniformly constructed with numerous nanorods radially grown on the surface of the carbon microspheres. Fig. 3b-c shows the morphology of the as-obtained $NiCo_2O_4$-carbon samples after calcination at 250 ℃ for 3 h. It can be observed that there appeared to be no noticeable structural change caused by the calcination process. However, the nanorods on the surface of the microsphere were obvious coarser after calcination, which is attributed to the thermal decomposition of the $NiCo_2O_4$-carbon precursors. Fig. 3d shows a typical rattle-type structural microsphere, which consists of a shell thickness of ca. 600 nm with carbon cores of ca. 1.2 μm in diameter.

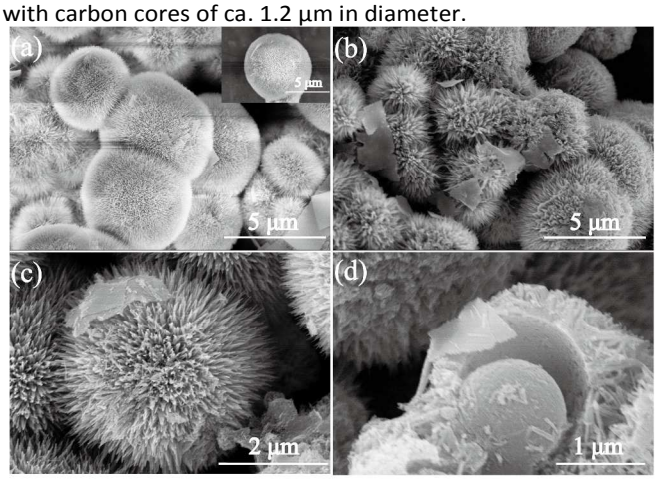

Fig. 3 SEM images of (a) $NiCo_2O_4$ precursor and (b-d) the as-prepared $NiCo_2O_4$-carbon composite microspheres after calcination at 250 ℃.

The detailed structure of the rattle-type $NiCo_2O_4$-carbon composite microspheres were further characterized by TEM. Fig. 4a shows a representative rattle-type structure, which is confirmed by the pale area marked in the ellipse. On the surface of the microspheres there are a lot of fine nanorods.

The high-magnification TEM image (Fig. 4b) clearly revealed the shell structure of the composite microsphere. It can be seen that the nanorods have high aspect ratios with a diameter of about 30 nm and a length of about 400 nm. And the nanorods were porous and composed of small nanoparticles. The connected-crystal structure of the nanoparticles was further characterized by HRTEM observations (Fig. 4c). The boundaries of the nanoparticles are clear on the atomic scale, and there are no amorphous layers covering the surface, which indicates the characteristics of the nanorods. It also can be seen that the lattice fringes with a d-spacing of 0.465 nm are clearly observed, which matches well with the (111) lattice spacing of $NiCo_2O_4$. The SAED pattern shows well-defined rings (Fig. 4d), indicating the polycrystalline characteristic crystal planes of $NiCo_2O_4$-carbon composite microspheres.

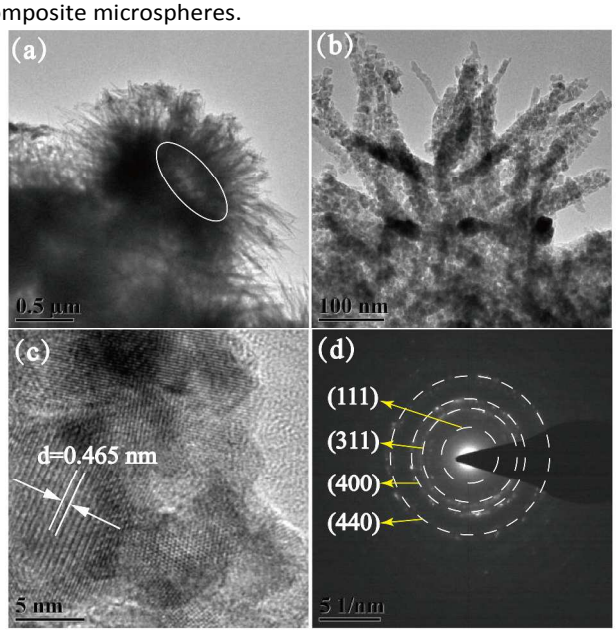

Fig. 4 (a) TEM, (b-c) HRTEM images and (d) SAED pattern of the rattle-type rattle-type $NiCo_2O_4$-carbon composite microsphere.

To investigate the effect of the calcination temperature on the product morphology, a series of experiments were carried out (Fig. S3). The Fig. S3a shows the prepared product calcinated at 300 ℃. It is clearly seen that the majority of the obtained product still show the urchin-like hierarchical structures with numerous nanorods radially grown on the surface. Some $NiCo_2O_4$ microspheres were collapsed, because the removal of carbon spheres lead to a loss of mechanical support for the $NiCo_2O_4$ nanoparticles. However, when the calcination temperature was up to 400 ℃, the majority of the prepared samples exhibit the network of spherical $NiCo_2O_4$ nanoparticles (Fig. S3b).

The porosity of the $NiCo_2O_4$ hierarchitectures is further investigated by the N_2 adsorption-desorption analysis, which is shown in Fig.5. The isotherms (Fig. 5a) exhibit characteristics of type-IV isotherms with an obvious hysteresis loop. The product also possesses a high specific surface area of 212.6 $m^2\ g^{-1}$ and a pore volume as high as 0.66 $cm^3\ g^{-1}$, respectively. The pore size distribution (the set in Fig.5a) of the product shows a sharp peak centred at 7.9 nm and a wide peak centred at 34.0 nm, respectively. The pores with a diameter of 7.9 nm mainly come from the assembly of $NiCo_2O_4$ nanorods. On the other hand, the pores with a diameter of 34.0 nm are mainly generated by the calcinated processes of the precursors[36, 37]. These features increase the active sites for the transport and diffusion of electrolyte ions during the charge–discharge process in supercapacitors, resulting in a greatly enhanced electrochemical activity. Fig. 5b shows the relationship between the calcination and specific surface area. The Brunauer-Emmett-Teller (BET) specific surface area of the products exhibits a remarkable decrease ranging from 123.5 to 96.7$m_2\ g^{-1}$, when the calcinated temperature increases from 250 ℃ to 400 ℃. The N_2 adsorption-desorption isotherms and corresponding pore size distribution of the samples calcinated at 300 and 400 ℃ were shown in Fig. S4.

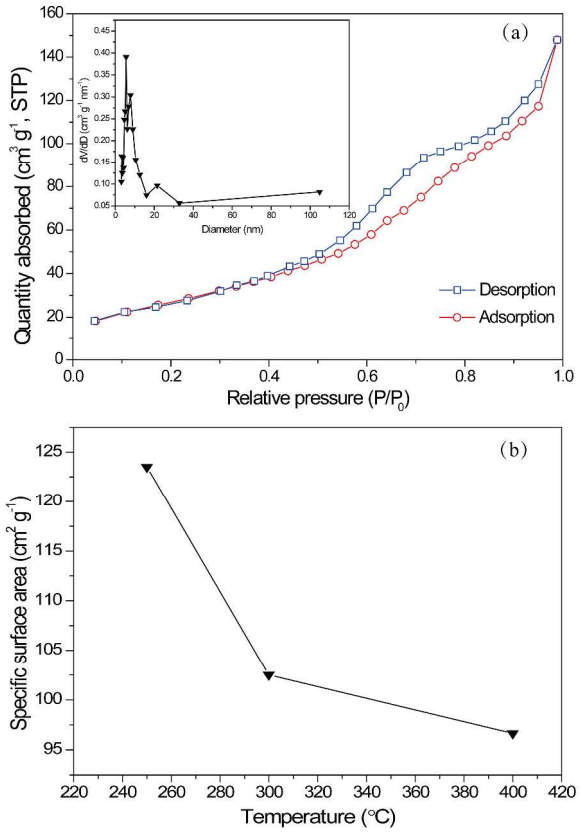

Fig. 5 (a) N_2 adsorption-desorption isotherms of the samples calcinated at 250 ℃: the inset is the corresponding pore size distribution; (b) the relationship plot of the calcination temperature and specific capacitance.

3.2. Electrochemical Characterization

The cyclic voltammetry (CV) curves of the obtained $NiCo_2O_4$ samples were recorded between 0 and 0.41 V at different scan rates ranging from 2 mV s^{-1} to 30 mV s^{-1} in 3 M KOH solution. As shown in Fig. 6a, it can be clearly seen that the CV curves consist of a pair of redox peaks, indicating the capacitive characteristics are mainly governed by Faradaic reaction[37]. The well-defined redox peaks mainly resulted from redox reactions of Ni and Co species in the alkaline electrolyte, as shown in the following equations[38]:

$$NiCo_2O_4 + OH^- + H_2O \leftrightarrow NiOOH + 2CoOOH + e^- \quad (5)$$

$$CoOOH + OH^- \leftrightarrow CoO_2 + H_2O + e^- \quad (6)$$

Interestingly, although two kinds of active centers for redox reaction from the solid state redox couples of Co^{2+}/Co^{3+} and Ni^{2+}/Ni^{3+} are present in the structures, there are no two couples of redox peaks of Co^{2+}/Co^{3+} and Ni^{2+}/Ni^{3+}. This phenomenon may be ascribed to the similar redox potential of Co_3O_4 and NiO and the surface modification of $NiCo_2O_4$ by conductive acetylene back which can induce appreciable broadening of some redox peaks[22]. Fig. 6d shows the comparison of the CV curves of the products obtained by calcination at different temperature at scan rate of 5 mV s^{-1}. Based on the fact that the area surround by the CV curve reflects the electrochemical performance of the electrode materials[39], it can be seen that the specific capacitance of the rattle-type $NiCo_2O_4$-carbon microsphere is much larger than that of the two other samples. This phenomenon can be attributed to the unique rattle-type structure of $NiCo_2O_4$-carbon composite microspheres, which favors faster ionic transport in the electrodes[33]. Besides, in comparison with the $NiCo_2O_4$-carbon composites, the samples calcinated at 300 and 400 ℃ have slightly shifted redox peaks in its CV plot, which can be ascribed to the different polarization behavior of the carbon in the rattle-type $NiCo_2O_4$-carbon microsphere[40].

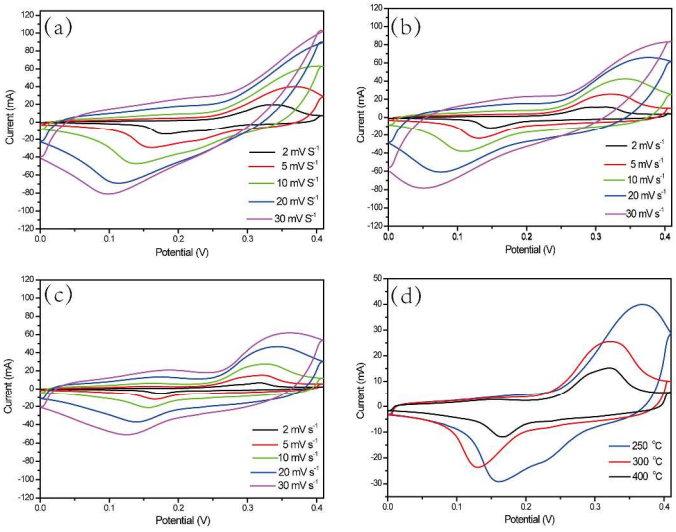

Fig. 6 CV curves of the $NiCo_2O_4$ products at a scan rate of 2, 5, 10, 20 and 30 mV s^{-1} between 0–0.41 V in 3 M KOH aqueous solution (a) 250 ℃, (b) 300 ℃ and (c) 400 ℃; (d) CVs of the $NiCo_2O_4$ samples at scan rates of 5 mV s^{-1}.

To further quantify the electrochemical properties of the calcinated samples, the galvanostatic CD measurements of the as-prepared $NiCo_2O_4$ samples were performed within a potential window of 0 to 0.41 V (vs. SCE). Fig. 7A shows the comparison of the CP plots of $NiCo_2O_4$ electrodes calcinated at different temperatures with a current density of 1 A g^{-1}. It can be calculated that the specific capacitance of the samples decreased from 790 F g^{-1} to 145 F g^{-1}, when the calcination temperature increase from 250 ℃ to 400 ℃, which is consistent with the results in Fig. 6d. The galvanostatic CD measurements of the rattle-type $NiCo_2O_4$-carbon composite microspheres were performed at various current densities of 1, 2, 4, 8 and 10 A g^{-1}. From the Fig. 7B, it can be seen that the nearly symmetric E-t curves at all current densities implies the high charge-discharge coulombic efficiency and low polarization of rattle-type $NiCo_2O_4$-carbon electrode[41]. Besides, because the redox reaction between Ni and Co cations and OH anions is a diffusion controlled process through electrode grain boundaries, the specific capacitance decreases as the current density increases[37]. Thus, with the increase of current density, the discharge time decreases.

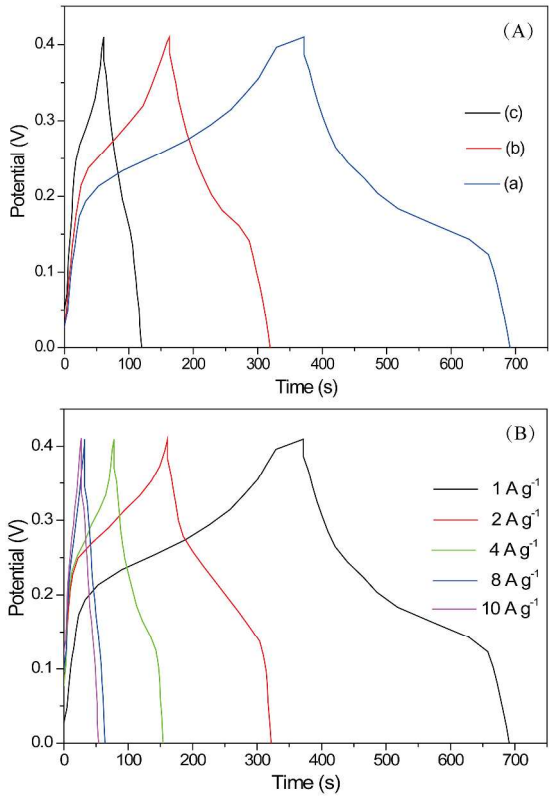

Fig. 7 (A) Comparison of the CP plots of $NiCo_2O_4$ electrodes calcinated at different temperatures at a current density of 1 A g^{-1}: (a) 250 ℃, (b) 300 ℃ and (c) 400 ℃. (B) CP plots of $NiCo_2O_4$ sample calcinated at 250 ℃ as a function of current density.

The specific capacitances of the unique rattle-type $NiCo_2O_4$-carbon electrode can be calculated based on the charge-discharge curves in Fig. 8b and the typical results are depicted in Fig. 8A. It can be seen that the specific capacitances of the rattle-type $NiCo_2O_4$-carbon electrode is evaluated to be 790, 770, 741, 624, and 609 F g^{-1} at current densities of 1, 2, 4, 8 and 10 A g^{-1}, respectively. This suggests that about 77.08 % of the capacitance is still retained when the charge-discharge rate is up to 10 A g^{-1} from 1 A g^{-1}. Ragone plots are also presented in Fig. 8B. When the power density increases from 205 W kg^{-1} (1 A g^{-1}) to 2050 W kg^{-1} (10 A g^{-1}), the corresponding energy density decreases from 18.4 Wh kg^{-1} to 14.2 Wh kg^{-1}. Based on the above results, we can conclude that the rattle-type $NiCo_2O_4$-carbon composite microsphere can be served as a promising electrode material for high-rate charge/discharge operations in supercapacitors[42].

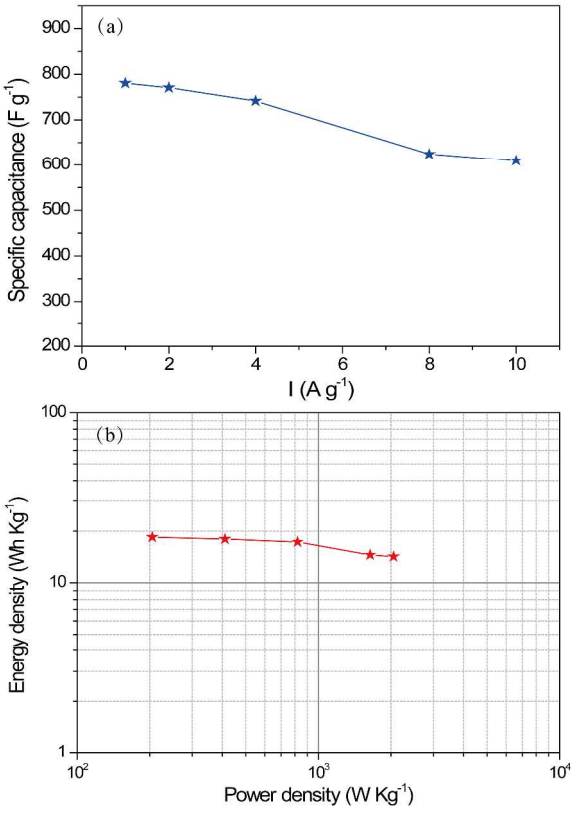

Fig. 8 (a) Calculated SC as a function of current density of the rattle-type $NiCo_2O_4$-carbon electrode; (b) Ragone plots of rattle-type $NiCo_2O_4$-carbon electrode.

Fig. 9 shows the Nyquist plots of the EIS spectra of rattle-type $NiCo_2O_4$-carbon electrode measured at an electrode potential of 0.30 V (vs. SCE). It can be seen that the rattle-type $NiCo_2O_4$-carbon electrode exhibits a small real axis intercept and negligible depressed semicircle in the high frequency range, suggesting small active bulk material resistance and a low interfacial resistance between current collector and active material, electrolyte resistance as well as low charge transfer resistance[31]. At lower frequencies, the oblique straight line represents the Warburg resistance (described as the diffusive impedence of OH^- ions) in electrode[43]. The rattle-type $NiCo_2O_4$-carbon electrode exhibits a vertical line leaning to imaginary axis more than 45°, indicating the more facile electrolyte ions diffusion to the active material due to its unique rattle-type structure.

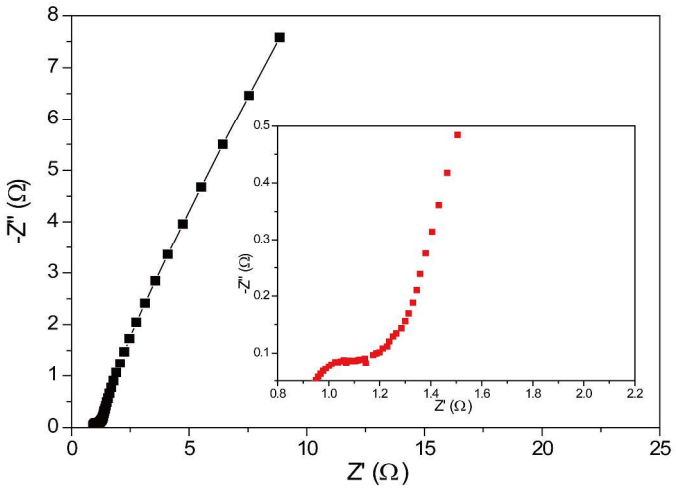

Fig. 9 Nyquist plot of the EIS of rattle-type $NiCo_2O_4$-carbon composite microspheres at 0.30 V (vs. SCE).

The long-term cycling stability and retention of the electrode materials during long charge-discharge cycles is also necessary to practical applications. Fig. 10 demonstrates the plots of specific capacitance and the retention of unique rattle-type $NiCo_2O_4$-carbon composite microspheres electrode for 2000 cycles under the current density of 2 A g^{-1}. Specially, the discharge capacity gradually increases up to 790 F g^{-1} in the first about 1500 cycles instead of decreasing as in most cycling stability tests, which might be ascribed to the full activation of the $NiCo_2O_4$-carbon composite material[34, 44]. More importantly, the decay in specific capacitance based on this maximum value after the following 500 cycle test is about 0.6 %, which may be ascribed to the volume change during the reaction process. And then the specific capacitance remains at a stable value of 775 F g^{-1} with further cycling. The excellent electrochemical stability was further confirmed by the inset galvanostatic CD curve of Fig. 10, which remains undistorted and essentially symmetric even after an extended period of charge and discharge cycles. These results confirm that rattle-type $NiCo_2O_4$-carbon electrode presents a large specific capacitances and excellent rate stability. Furthermore, the coulombic efficiency keeps at about 100% during the consecutive cycles.

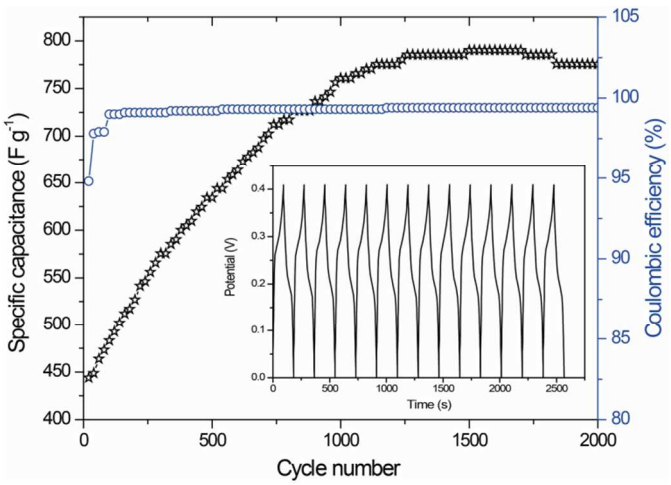

Fig. 10 Specific discharge capacity and coulombic efficiency of the rattle-type $NiCo_2O_4$-carbon electrode tested for 2000 cycles at a current density of 2 A g^{-1}; the inset shows charge–discharge curves in potential range from 0 to 0.41 V.

The excellent electrochemical performance of the rattle-type $NiCo_2O_4$-carbon composite microspheres could be ascribed to the following factors. Firstly, the higher electronic conductivity of the mixed spinel $NiCo_2O_4$ is beneficial to the repaid ion or electron transfer at the electrode/electrolyte interface[42]. Secondly, the high specific area and rattle-type feature of the $NiCo_2O_4$-carbon composite microspheres reduce the diffusion length of electrolyte ions and ensure enough electrolyte ions to rapidly contact the $NiCo_2O_4$ with rich electroactive sites. In particular, the void between the carbon core and $NiCo_2O_4$ shell can serve as "ion-buffering reservoirs" to efficiently hold OH^- ions for the sufficient Faradaic reactions.

4. Conclusions

In summary, we developed an efficient template-engaged synthetic strategy to fabricate rattle-type $NiCo_2O_4$-carbon composite microspheres. When utilized as an appealing electroactive material for supercapacitors, the as-fabricated rattle-type $NiCo_2O_4$-carbon electrode delivered high specific capacitance and high-rate capacity (780 F g^{-1} at 1 A g^{-1}, 78.01% retention at 10 A g^{-1}). Furthermore, desirable cycling stability of 0.6% SC loss after continuous 2000 cycles at 2 A g^{-1} was observed, suggesting their promising application in supercapacitors. Further experiments demonstrate that the calcination temperature plays an important role in the morphology and electrochemical performance. More significantly, the electrode design concept can be easily generalized to other binary or even ternary metal oxides with unique rattle-type nano/microstructures for high performance supercapacitors, or even advanced Li-ion batteries.

Acknowledgements

This work is financially supported by Science and Technology Development Plan of Shandong Province, China (2014GNC110013), the National Natural Science Foundation for Young (No. 2130696) and Graduate Innovation Fund of Qingdao Agricultural University (QYC201422).

Notes and references

[a] Qingdao Agricultural University, Qingdao 266109, People's Republic of China.

1. Z. Xu, C. Li, G. Li, R. Chai, C. Peng, D. Yang and J. Lin, *The Journal of Physical Chemistry C*, 2010, 114, 2573.
2. H. B. Wu, A. Pan, H. H. Hng and X. W. D. Lou, *Advanced Functional Materials*, 2013, 23, 5669.
3. H. Lin, L. Li, M. Zhao, X. Huang, X. Chen, G. Li and R. Yu, *Journal of the American Chemical Society*, 2012, 134, 8328.
4. T.-T. Wang, F. Chai, C.-G. Wang, L. Li, H.-Y. Liu, L.-Y. Zhang, Z.-M. Su and Y. Liao, *Journal of Colloid and Interface Science*, 2011, 358, 109.
5. Y. P. Xie, Z. B. Yu, G. Liu, X. L. Ma and H.-M. Cheng, *Energ Environ Sci*, 2014, 7, 1895.
6. H.-S. Lim, Y.-K. Sun and K.-D. Suh, *Journal of Materials Chemistry A*, 2013, 1, 10107.
7. L. Wang, T. Fei, J. Deng, Z. Lou, R. Wang and T. Zhang, *Journal of Materials Chemistry*, 2012, 22, 18111.
8. L. Wang, Z. Lou, T. Fei and T. Zhang, *Journal of Materials Chemistry*, 2011, 21, 19331.
9. Z. Xu, P. Ma, C. Li, Z. Hou, X. Zhai, S. Huang and J. Lin, *Biomaterials*, 2011, 32, 4161.
10. D. Wang, H. Zhang, J. Guo, H. Xu, X. Zhu and Z. Jiao, *RSC Advances*, 2014, 4, 37311.
11. T. Okada, S. Ozono, M. Okamoto, Y. Takeda, H. M. Minamisawa, T. Haeiwa, T. Sakai and S. Mishima, *Ind Eng Chem Res*, 2014, 53, 8759.
12. X. Wang, X. L. Wu, Y. G. Guo, Y. Zhong, X. Cao, Y. Ma and J. Yao, *Advanced Functional Materials*, 2010, 20, 1680.
13. G. Q. Zhang, H. B. Wu, H. E. Hoster, M. B. Chan-Park and X. W. Lou, *Energ Environ Sci*, 2012, 5, 9453.
14. R. Liu, L. Wan, S. Liu, L. Pan, D. Wu and D. Zhao, *Advanced Functional Materials*, 2015, 25, 526.
15. M.-C. Liu, L.-B. Kong, C. Lu, X.-M. Li, Y.-C. Luo and L. Kang, *ACS applied materials & interfaces*, 2012, 4, 4631.
16. B. Wang, T. Zhu, H. B. Wu, R. Xu, J. S. Chen and X. W. Lou, *Nanoscale*, 2012, 4, 2145.
17. H. B. Wu, H. Pang and X. W. Lou, *Energ Environ Sci*, 2013, 6, 3619.
18. Y. Zhu, Z. Wu, M. Jing, W. Song, H. Hou, X. Yang, Q. Chen and X. Ji, *Electrochimica Acta*, 2014, 149, 144.
19. B. Kaur, B. Satpati and R. Srivastava, *New J Chem*, 2015, 39, 1115.
20. Q. Wang, B. Liu, X. Wang, S. Ran, L. Wang, D. Chen and G. Shen, *Journal of Materials Chemistry*, 2012, 22, 21647.
21. Y. Zhu, Z. Wu, M. Jing, H. Hou, Y. Yang, Y. Zhang, X. Yang, W. Song, X. Jia and X. Ji, *Journal of Materials Chemistry A*, 2015, 3, 866.
22. Y. Lei, J. Li, Y. Wang, L. Gu, Y. Chang, H. Yuan and D. Xiao, *ACS applied materials & interfaces*, 2014, 6, 1773.
23. J. Du, G. Zhou, H. Zhang, C. Cheng, J. Ma, W. Wei, L. Chen and T. Wang, *ACS applied materials & interfaces*, 2013, 5, 7405.
24. Y. Zhu, J. Wang, Z. Wu, M. Jing, H. Hou, X. Jia and X. Ji, *Journal of Power Sources*, 2015, 287, 307.
25. R. Ding, L. Qi and H. Wang, *J Solid State Electr*, 2012, 16, 3621-3633.
26. Y. Zhu, X. Ji, Z. Wu, W. Song, H. Hou, Z. Wu, X. He, Q. Chen and C. E. Banks, *Journal of Power Sources*, 2014, 267, 888.
27. X. Sun and Y. Li, *Angewandte Chemie International Edition*, 2004, 43, 597.
28. X. Yu, B. Lu and Z. Xu, *Advanced Materials*, 2014, 26, 1044.
29. S. K. Meher and G. R. Rao, *The Journal of Physical Chemistry C*, 2011, 115, 15646.
30. Y. Sun, L. Zhang, J. Zhang, P. Chen, S. Xin, Z. Li and J. Liu, *Ceramics International*, 2014, 40, 1599.
31. Y. Zhu, X. Pu, W. Song, Z. Wu, Z. Zhou, X. He, F. Lu, M. Jing, B. Tang and X. Ji, *J Alloy Compd*, 2014, 617, 988.
32. S.-I. Kim, J.-S. Lee, H.-J. Ahn, H.-K. Song and J.-H. Jang, *ACS applied materials & interfaces*, 2013, 5, 1596.
33. Y. N. Ko, Y. C. Kang and S. B. Park, *RSC Advances*, 2014, 4, 17873.
34. J. Pu, J. Wang, X. Jin, F. Cui, E. Sheng and Z. Wang, *Electrochimica Acta*, 2013, 106, 226.
35. Y. Q. Wu, X. Y. Chen, P. T. Ji and Q. Q. Zhou, *Electrochimica Acta*, 2011, 56, 7517.

36. Z. Xingfu, H. Zhaolin, F. Yiqun, C. Su, D. Weiping and X. Nanping, *The Journal of Physical Chemistry C*, 2008, 112, 11722.
37. Y. Zhang, M. Ma, J. Yang, H. Su, W. Huang and X. Dong, *Nanoscale*, 2014, 6, 4303.
38. X. Liu, S. Shi, Q. Xiong, L. Li, Y. Zhang, H. Tang, C. Gu, X. Wang and J. Tu, *ACS applied materials & interfaces*, 2013, 5, 8790.
39. H. Xia, C. Hong, B. Li, B. Zhao, Z. Lin, M. Zheng, S. V. Savilov and S. M. Aldoshin, *Advanced Functional Materials*, 2015, 25, 627.
40. W. Zhou, D. Kong, X. Jia, C. Ding, C. Cheng and G. Wen, *Journal of Materials Chemistry A*, 2014, 2, 6310.
41. C. Yuan, J. Li, L. Hou, J. Lin, G. Pang, L. Zhang, L. Lian and X. Zhang, *RSC Advances*, 2013, 3, 18573.
42. H. Jiang, J. Ma and C. Li, *Chem Commun*, 2012, 48, 4465.
43. M.-C. Liu, L.-B. Kong, C. Lu, X.-M. Li, Y.-C. Luo, L. Kang, X. Li and F. C. Walsh, *Journal of The Electrochemical Society*, 2012, 159, A1262.
44. Z. Zhu, J. Ping, X. Huang, J. Hu, Q. Chen, X. Ji and C. Banks, *J Mater Sci*, 2012, 47, 503.